JOURNAL OF COMPUTATIONAL PHYSICS **138,** 665–694 (1997)
ARTICLE NO. CP975840

Pseudospectral/Delves–Freeman Computations of the Radiation Coefficient for Weakly Nonlocal Solitary Waves of the Third-Order Nonlinear Schroedinger Equation and Their Relation to Hyperasymptotic Perturbation Theory

John P. Boyd

Department of Atmospheric, Oceanic & Space Sciences, University of Michigan, 2455 Hayward Avenue, Ann Arbor, Michigan 48109

Received October 2, 1996

We revive a strategy of Delves to precondition a spectral calculation using an almost-diagonal Galerkin matrix. We also show that hyperasymptotic singular perturbation theory is a specialization of the Delves–Freeman iteration to a single step with a diagonal Galerkin matrix. We calculate the first three orders in the hyperasymptotic expansion of the radiation coefficient of the weakly nonlocal envelope solitary waves of the third-order nonlinear Schroedinger (TNLS) equation, which is important in fiber optics telecommunications and water waves. In a long appendix, it was necessary to develop some non-numerical but numerically essential additions to the theory of the TNLS equation: Good numerics often requires a much deeper understanding of a problem than the generation of a string of power series coefficients.

1. INTRODUCTION

Our goal is to compute spatially periodic solutions to the nonlinear boundary value problem

$$-\frac{1}{2}\varepsilon^2 Q + i\varepsilon^2 Q_x + \frac{1}{2}Q_{xx} + |Q|^2 Q - iQ_{xxx} = 0. \tag{1.1}$$

Each branch of periodic solutions is a two-parameter family where the constant ε

0021-9991/97 $25.00

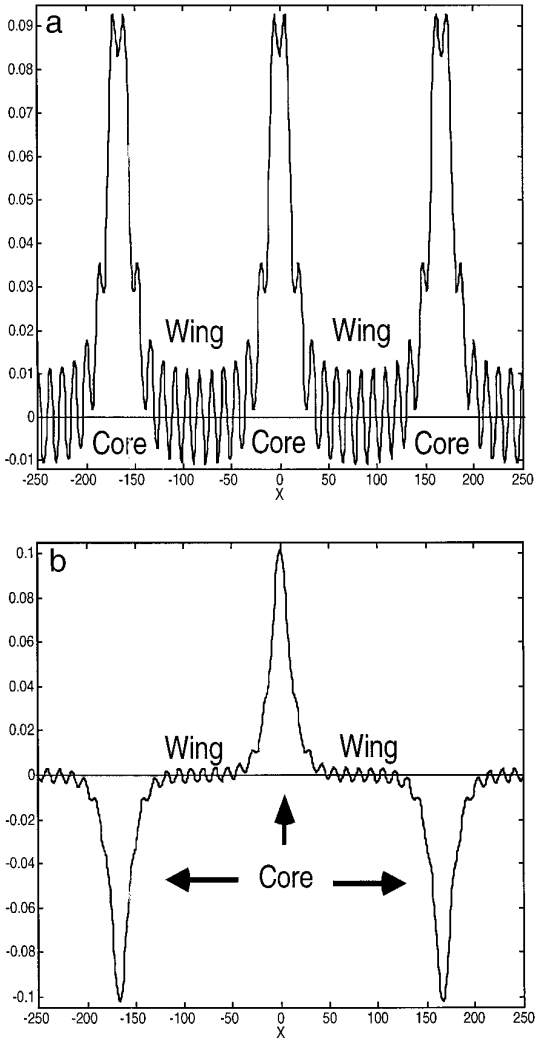

FIG. 1. (a) TNLS nanopteroidal wave, dnoidal-like branch. Re($Q(X)$) is graphed for $\varepsilon = 1/10$ and a spatial period of 333.323. (b) Same as (a) except the cnoidal-like branch is illustrated.

and the spatial period P are the parameters. (By convention, $\varepsilon > 0$ and this will be implicitly assumed throughout the rest of the article.) The parameter $\varepsilon \ll 1$ for the calculations described here. When $\varepsilon \ll 1$, the solutions are dominated by a ''core'' peak on each period which is approximately

$$Q \sim \pm\varepsilon\,\mathrm{sech}(\varepsilon X), \qquad \varepsilon \ll 1. \tag{1.2}$$

However, the large peaks or troughs do not decay to zero but rather to oscillatory wings of amplitude $\alpha(\varepsilon; P)$ (Fig. 1). The waves are said to be ''weakly nonlocal'' [7–10].

Equation (1.1) is the stationary form of the third-order nonlinear Schroedinger

TABLE I
A Selected Bibliography of Weakly Nonlocal Envelope Solitary Waves

Reference	Equation	Remarks
11	TNLS	Initial value solutions; observed one-sided radiative decay
1	TNLS	Double-humped solitons with $\alpha = 0$ (''bions''); connection with wave caustics and Eckhart resonances in internal water waves; nanopteroidal waves
12	TNLS	Complex plane matched asymptotics
13	TNLS	Computation of α through conservation laws and self-consistent iteration in Fourier space
14	TNLS	Dark solitons in the normal dispersion regime
15, 16	TNLS	Inverse scattering-based perturbation theory
17	TNLS	Theoretical analysis of bions and other bound states of nonlocal envelope solitons
18	TNLS	Numerical computation of bions for the discrete parameters for which $\alpha = 0$; applications in fiber optics
19	TNLS	Simplified and heuristic evaluation of α up to an $O(1)$ multiplier
20	TNLS	Modulational (''sideband'') instability and recurrence
21, 22	MB	Computes the discrete parameter values where $\alpha = 0$ so that a classical soliton exists.
23	Lattice–KG	Derives NLS, coupled pair of NLS, and TNLS models for waves on a lattice
24	KG	Numerical
25	TNLS	Hyperasymptotics
26	TNLS	Complex-plane matched asymptotics
27	TNLS	Construction of bound states by matched asymptotic expansions

Note. TNLS, third-order cubic Schroedinger equation; MB, Maxwell–Block equations of self-induced transparency; KG, Klein–Gordon equation.

equation (TNLS) which describes the envelope of nonlinear wave packets. It differs from the nonlinear Schroedinger (NLS) equation only through the presence of the third derivative.

The TNLS equation and closely related equations that also describe ''weakly nonlocal'' envelope solitary waves have been studied by many authors (Table 1). Akylas and Kung [1] apply this equation to describe caustics and Eckhart resonances in internal waves, and note that envelope solitons have been observed in ship wakes [2].

Envelope solitons, modelled by either the NLS or the TNLS equation, may carry digital signals in fiber optics for long distance telecommunication. Glass [3] predicts that ''solitons, with all of their advantages, are expected to find their way into commercial systems before the end of the decade.'' Good reviews of solitons-in-fiber are also given by Hasegawa [4], Drummond *et al.* [5], and Desurvire [6]. Optical solitons of minimal energy occur for wavelengths on the boundary between ''regular'' and ''anomalous'' dispersion. This parametric region is precisely where the NLS equation must be replaced by the TNLS equation.

The TNLS equation has two families of periodic solutions with one large peak or trough on each spatial period (Fig. 1). By analogy with the corresponding solutions of the NLS equations, these may be dubbed the ''dnoidal'' and ''cnoidal'' families of solutions. The dnoidal family has core peaks which are all positive whereas the cores of the cnoidal branch alternate peaks and troughs. Because the solutions for both families are very similar when the spatial period P is large compared to the width of the core, as will always be assumed here, we shall solve only for the dnoidal family.

The limit that the spatial period $P \Rightarrow \infty$ yields a ''weakly nonlocal solitary'' wave or ''nanopteron.'' This has only a single large peak (or trough) plus oscillatory wings filling all of space. When P is large, the spatially periodic solutions agree with the nonlocal soliton to within an error that decreases exponentially with P on the interval $X \in [-P/2 + \delta, P/2 - \delta]$ where δ is small compared to P but otherwise arbitrary. Consequently, we can compute the nanopteron by computing its spatially periodic generalization (''nanopteroidal wave'') instead.

Spatially periodic solutions are of some physical interest in and of themselves. However, in this article the primary goal will be to compute nanopterons (on the infinite interval) by calculating spatially periodic solutions which approximate the infinite interval solutions of the same differential equation (1.1) with the same parameter ε.

In place of the spatial period P, the nanopteron has a degree of freedom Φ, the ''far field phase factor,'' which controls the amplitude and phase of the wing oscillations without having much effect on the core. For nanopteroidal waves, the spatial period P is equivalent to the phase parameter Φ for the equivalent nanopteron; the far field phase Φ must take a definite value $\Phi(P)$ so that the oscillations radiating from the core centered at $X = 0$ will match smoothly to the oscillations radiating from the neighboring core at $X = P$. The physically interesting Φ is that which *minimizes* the amplitude of the wing oscillations for a given amplitude of the core ε [26, 10].

To obtain this relationship between Φ and P, it is necessary to compute the eigenfunctions of the linearized form of (1.1) as done in Appendix B. For the numerical problem of solving (1.1), the only purpose of the eigenfunction analysis is to furnish the physically interesting spatial period P.

Singular perturbation theories show that the minimum amplitude of the oscillatory wings for a given ε is of the form [12, 26]

$$\alpha_{\min}(\varepsilon) \sim \nu_0(1 + \nu_1\varepsilon + \nu_2\varepsilon^2 + \cdots) \exp\left(-\frac{\pi}{4\varepsilon}\right), \qquad \varepsilon \ll 1. \tag{1.3}$$

Unfortunately, determining the constants ν_0, ν_1, ν_2, etc., is very difficult. The leading constant has been calculated by several groups [12, 26], always by a mixture of analytical approximations and numerical work. (It seems to be well-nigh impossible to obtain a closed-form approximation to ν_0, for this or any other case of ''weakly nonlocal solitary waves.'') In this work, we obtain the next two terms by solving the nonlinear boundary value problem to very high accuracy using a Fourier–Galerkin method and then fitting the results to the form of Eq. (1.3).

We have been obliged to inflict all this background about nonlocal solitary waves on the reader because the TNLS physics greatly challenges the numerical algorithm. First, the spatial period P must be large compared to $1/\varepsilon$, or otherwise the exponentially decaying tail of one core peak will overlap that of its nearest neighbor so as to swamp the wing oscillations and destroy the approximation of the nanopteron by its spatially periodic generalization. Second, the problem is nonlinear and contains two disparate spatial scales ($1/\varepsilon$ and P). Third, it must be solved to very high accuracy. The reason is that $\alpha_{\min}$ decays *exponentially* fast as $\varepsilon \Rightarrow 0$, so a solution for $\varepsilon = 1/20$ has wing oscillations which are a thousand trillion times smaller than the amplitude of the core!

A Fourier spectral method can provide the needed accuracy with a modest number of degrees of freedom N. Furthermore, we can exploit the symmetries of (1.1)—the real part of the solution is symmetric with respect to $X = 0$ while the imaginary part is of antisymmetric parity—to halve N. However, we still need $N > 1000$, and the Fourier collocation and Galerkin matrices are dense matrices with almost every element nonzero.

The best way to reduce cost is to replace Newton's iteration by a quasi-Newton scheme. By using fast Fourier transforms, the residual, which is the result of substituting the current iterate into the differential equation, can be evaluated in only $O(N \log_2(N))$ operations. The costly step is computing the LU factorization of the Jacobian matrix, which is the spectral discretization of the linearization of the nonlinear equation with respect to the current iterate. The Jacobian matrix requires $O(N^2)$ storage and its factorization costs about $O([2/3]\, N^3)$ operations. The key is to approximate the dense Jacobian matrix by a sparse matrix which is an order of magnitude cheaper to store and factorize.

The usual strategy is to approximate the Jacobian matrix by a finite difference or finite element discretization of the same linearized differential equation [29–32]. This "finite difference preconditioning" requires that the spectral residual must be transformed to the points of an associated interpolation grid so that the underlying algorithm is a pseudospectral or collocation scheme.

In this work, we approximate (or "precondition") the Jacobian matrix in a Galerkin framework by using an "almost diagonal" Fourier–Galerkin matrix. In this scheme, developed by Delves [38] and Delves and Freeman [28], all off-diagonal matrix elements, except a few that couple the "important" modes, are discarded to create the preconditioner. In most applications, the "important" modes are simply those of low degree. Here, however, there is a resonance between high wavenumber and low wavenumber which is responsible for the oscillatory wings. The resonance implies that the Fourier modes whose wavenumbers approximately match those of the wings may be "important," too. In any event, neglecting all but the low-or-resonant wavenumbers gives a sparse approximate Galerkin matrix which is cheap to factor. We shall show below that the quasi-Newton iteration still converges rapidly. Because no approximations are made in evaluating the *residual*, the Delves–Freeman iteration converges to an answer which is accurate to full spectral accuracy, the same as if one had used an "honest" Newton's method that calculated and factored a dense Jacobian matrix at each iteration.

2. THE FOURIER–GALERKIN ALGORITHM

Because the solutions are spatially periodic, the sines and cosines of an ordinary Fourier series are the most efficient basis functions. As explained in Appendix A, all solutions computed here have the property that the real part of $Q(X)$ is symmetric with respect to X and the imaginary part is antisymmetric. With this symmetry assumption, nanopteroidal waves can be computed through the Fourier expansion

$$Q(X) = \sum_{j=0}^{N-1} a_j \cos(jX/L) + i \sum_{j=1}^{N} b_j \sin(jX/L), \tag{2.1}$$

where the spatial period $P = 2\,\pi\,L$ and where the cosine and sine coefficients are *real*. (Asymmetric solutions, perhaps with multiple cores of slightly different sizes, may well exist; to compute them, it is only necessary to include sines and cosines for both the real and imaginary parts.) Writing $Q = Q_r + iQ_{im}$, the reduced TNLS equation (1.1) can be reduced to the coupled pair of real-valued equations:

$$\begin{aligned} -\tfrac{1}{2}\varepsilon^2 Q_r - \varepsilon^2 Q_{im,X} + \tfrac{1}{2}Q_{r,XX} + (Q_r^2 + Q_{im}^2)Q_r + Q_{im,XXX} = 0 \\ -\tfrac{1}{2}\varepsilon^2 Q_{im} + \varepsilon^2 Q_{r,X} + \tfrac{1}{2}Q_{im,XX} + (Q_r^2 + Q_{im}^2)Q_{im} - Q_{r,XXX} = 0. \end{aligned} \tag{2.2}$$

The Newton–Kantorovich iteration to solve these is

$$J(Q^{(m)})\,\Delta^{(m)} = -r(Q^{(m)}), \qquad Q^{(m+1)} = Q^{(m)} + \Delta^{(m)}, \tag{2.3}$$

where the inhomogeneous linear differential equation is solved repeatedly until the correction Δ is sufficiently small. The Jacobian operator J is the linearization of the system (2.2) with respect to the current iterate,

$$J(Q)\,\Delta \equiv \begin{cases} -\tfrac{1}{2}\varepsilon^2\,\Delta_r - \varepsilon^2\,\Delta_{im,X} + \tfrac{1}{2}\Delta_{r,XX} + (3Q_r^2 + Q_{im}^2)\,\Delta_r + 2Q_rQ_{im}\,\Delta_{im} + \Delta_{im,XXX} \\ -\tfrac{1}{2}\varepsilon^2\,\Delta_{im} + \varepsilon^2\,\Delta_{r,X} + \tfrac{1}{2}\Delta_{im,XX} + (Q_r^2 + 3Q_{im}^2)\,\Delta_{im} + 2Q_rQ_{im}\,\Delta_r - \Delta_{r,XXX} \end{cases}, \tag{2.4}$$

and the residual is the result of substituting the previous iterate into the differential equation

$$r(Q) \equiv \begin{cases} -\tfrac{1}{2}\varepsilon^2\,Q_r - \varepsilon^2 Q_{im,X} + \tfrac{1}{2}Q_{r,XX} + (Q_r^2 + Q_{im}^2)Q_r + Q_{im,XXX} \\ -\tfrac{1}{2}\varepsilon^2\,Q_{im} + \varepsilon^2 Q_{r,X} + \tfrac{1}{2}Q_{im,XX} + (Q_r^2 + Q_{im}^2)Q_{im} - Q_{r,XXX} \end{cases} \tag{2.6}$$

The residual can be evaluated in $O(N\,\log_2(N))$ operations by the fast Fourier transform [29, 31, 33]. The Galerkin integrals were approximated by numerical quadrature with the number of grid points equal to the number of unknowns (of each symmetry) although more points could be used if desired).

The differential equation is discretized by Galerkin's method to $\vec{\vec{J}}\vec{\Delta} = \vec{r}$ where the matrix elements are

$$J_{ij} = (\phi_i, J(Q)\phi_j), \qquad r_i = (\phi_i, r(Q)). \tag{2.7}$$

The elements of the column vector $\vec{\Delta}$ are the Fourier coefficients of the correction. The parentheses denote the L_2 inner product, which is the integral of the product of the factors inside the parentheses on the interval $x \in [0, P/2]$. (Because of the symmetry, it is sufficient to integrate over half the spatial period.) The basis functions are

$$\phi_{2j}(x) = \cos(jx), j = 0, 1, ..., N/2 - 1; \qquad \phi_{2j-1}(x) = \sin(jx), j = 1, 2, ..., N/2. \tag{2.8}$$

The iteration requires a first guess. The lowest perturbative approximation

$$Q^{(0)}(X) = \varepsilon \operatorname{sech}(\varepsilon X) \tag{2.9}$$

was always a sufficiently good guess that Newton's iteration converged.

Two major technical problems remain. The first is that the factorization of the dense Jacobian matrix is very expensive. It is possible to enormously reduce the cost by using the Delves–Freeman iteration (next section).

The second problem is peculiar to weakly nonlocal solitary waves: What choice of spatial period P for the Fourier computation yields good approximations to the infinite interval solutions of physical interest, which are those which have the smallest oscillatory "wings"? This question is answered by the eigenfunction analysis of Appendix B. We have banished this to an appendix because, to solve the numerical problem, we need only the result: the spatial period P. Actually, an infinite set of discrete periods P are suitable, each differing from one another through an *integral* multiple of the wavelength of the "wings" of the nanopteron.

3. THE DELVES–FREEMAN ITERATION

Delves [38] developed a fast iteration scheme which is explained at length in the monograph by Delves and Freeman [28]. The key idea is most easily explained by using a simple example which is not directly related to the TNLS equation,

$$u_{xx} + Q(x)u = f(x), \tag{3.1}$$

with the boundary condition that $u(x)$ is periodic with period 2π where $|Q(x)|$ is bounded by a constant which for simplicity will be assumed to be one. To simplify the analysis further, assume that $Q(x)$ and $f(x)$ and therefore $u(x)$ are all symmetric with respect to the origin so that the solution is a cosine series (as opposed to a general Fourier series). The Fourier–Galerkin representation of (3.1) is then the matrix problem

$$\vec{\vec{L}}\vec{a} = \vec{f}, \tag{3.2}$$

where the elements a_j and f_j of the column vectors $\vec{a}$ and $\vec{f}$ are the Fourier coefficients of the unknown $u(x)$ and the forcing function $f(x)$,

$$u(x) = \sum_{j=0} a_j \cos(jx), \qquad f(x) = \sum_{j=0} f_j \cos(jx), \tag{3.3}$$

and where the elements of the dense square matrix $\vec{\vec{L}}$ are

$$L_{ij} = \frac{2}{\pi} \int_0^\pi \cos(ix) \left\{ \frac{d^2}{dx^2} \cos(jx) + Q(x) \cos(jx) \right\}. \tag{3.4}$$

Delves and Freeman note that $\vec{\vec{L}}$ is the sum of two simpler matrices: one whose elements are the inner products of the basis functions with the second derivatives of the basis functions and the other which is the inner product of pairs of basis functions with $Q(x)$. The critical point is that because the second derivative of $\cos(jx)$ is simply $-j^2 \cos(jx)$ and because the cosines are orthogonal, the Galerkin matrix for the second derivative is *diagonal,*

$$L_{ij} = D_{ij} + Q_{ij} \tag{3.5a}$$

$$D_{ij} = -j^2 \, \delta_{ij} \tag{3.5b}$$

$$Q_{ij} = \frac{2}{\pi} \int_0^\pi \cos(ix) Q(x) \cos(jx) \, dx, \tag{3.5c}$$

where δ_{ij} is the usual Kronecker delta function, equal to one when its subscripts are equal and zero otherwise.

If the matrix $\vec{\vec{L}}$ were really diagonal, then

$$a_j = f_j / L_{jj}. \tag{3.6}$$

Unfortunately, the matrix is actually the worst possible case, a dense matrix, because of the Q_{ij}. However, our assumption that $Q(x)$ is bounded by unity implies

$$|Q(x)| \le 1 \Rightarrow |Q_{ij}| \le \frac{2}{\pi}. \tag{3.7}$$

However, the elements of the diagonal matrix $\vec{\vec{D}}$ are growing as

$$D_{jj} = -j^2. \tag{3.8}$$

It follows that as j increases, the jth row and the jth column of the full matrix $\vec{\vec{L}}$ will be more and more dominated by the diagonal element.

Unfortunately, this is not necessarily true for small j where both the diagonal and off-diagonal elements are the same order. The proper assertion is that the Fourier–Galerkin matrix is "weakly asymptotically diagonal" in the sense defined by Delves and Freeman [28]. This means that the jth row and column is not necessarily dominated (in magnitude and importance) by L_{jj} for *all* j, but this dominance develops with increasing strength in the *asymptotic limit* $j \Rightarrow \infty$.

Thus, Delves [38] approximated the Galerkin matrix by a matrix composed of the *diagonal* plus a *full upper left block.* The dense block accounts for those few

rows and columns where the off-diagonal and diagonal elements are the same order of magnitude. The elements of the approximating matrix $\vec{\vec{L}}^{(\text{approx})}$ are

$$L_{ij}^{(\text{approx})} \equiv \begin{cases} L_{ij}, & i \le N_D \text{ and } j \le N_D \\ \delta_{ij} L_{ij}, & i \text{ and/or } j > N_D \end{cases}. \tag{3.9}$$

The size of the $N_D \times N_D$ block is user-choosable; the larger the block, the better the approximation of $\vec{\vec{L}}$, but the greater the cost,

$$\text{LU factorization of } \vec{\vec{L}}^{(\text{approx})} \approx (2/3)N_D^3 + O(N) \text{ floating point operations}, \tag{3.10}$$

where N is the truncation of the Fourier–Galerkin matrix and therefore the dimension of both $\vec{\vec{L}}$ and $\vec{\vec{L}}^{(\text{approx})}$.

If $N_D \ll N$, then the cost of solving a matrix equation with a block-and-diagonal matrix is only a little more than that of a diagonal matrix. The critical question is, If the Jacobian is approximated by such a block-and-diagonal matrix, does the iteration still converge?

The answer is yes—if the block is sufficiently large. The quadratic convergence of Newton's iteration is lost, as it is in any procedure that is only quasi-Newton. However, the convergence of the Delves–Freeman iteration is geometric with the error decreasing by roughly a constant factor at each iteration.

This example (3.1) is discussed at length with graphs and tables in the author's book [29]. The application to the TNLS equation is very similar, but there are a couple of interesting complications.

The first is that the TNLS solution is a sum of both sines and cosines. The odd derivatives of $\sin(jx)$ are cosines and therefore contribute to the rows of the Galerkin matrix where we multiply on the left by $\cos(ix)$. However, the even derivatives of $\sin(jx)$ are sines and contribute to the rows where we multiply by $\sin(ix)$. Thus, the linear constant coefficient terms in the differential equation strongly couple the rows and columns corresponding to sines and cosines of the same row number. If we order the unknowns properly, then the linear constant coefficient terms define a Fourier–Galerkin matrix which has 2×2 blocks on the main diagonal. Figure 2 shows the nonzero elements for such a matrix, which we shall refer to as the "bidiagonal" matrix.

Thus, the Delves–Freeman matrix $\vec{\vec{L}}^{(\text{approx})}$ has the block-plus-bidiagonal structure illustrated in Fig. 3. However, the bidiagonal matrix can be solved in $O(N)$ operations, so the cost estimate (3.10) still applies.

The second complication is that in the "far field," that is, $|X| \gg 1$ where the nonlinear term in the TNLS equation can be neglected, the linear terms cancel for wavenumber $K = -1/2$ so that $\exp(-iX/2)$ is an approximate solution of the differential equation. For the Fourier basis with $\{\cos(jX/L), \sin(jX/L)\}$ as the basis functions, this implies that for mode number j close to

$$j_{\text{res}} \equiv L/2 \tag{3.11}$$

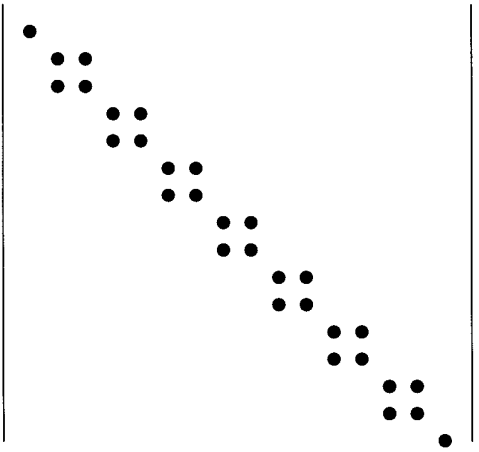

FIG. 2. Schematic of the nonzero matrix elements (disks) of the bidiagonal matrix which is the Fourier–Galerkin discretization of the linear terms in the TNLS equation.

the bidiagonal matrix will have small eigenvalues and will not dominate the matrix elements of the linearized nonlinear terms in the TNLS equation, which are analogous to the Q_{ij} for (3.1). This suggests that it may be necessary to generalize the Delves–Freeman strategy by also retaining rows and columns of the matrix for basis functions such that $j \approx j_{\text{res}}$.

Surprisingly, however, the Delves–Freeman iteration works well for the TNLS equation even *without* special treatment of the near-resonant basis functions. Figure 4 is the norm of the residual versus the iteration number. On this log/linear plot, geometric convergence is a curve that asymptotes to a constant linear slope. Newton's iteration, which is a full recomputation and factorization of the dense, un-

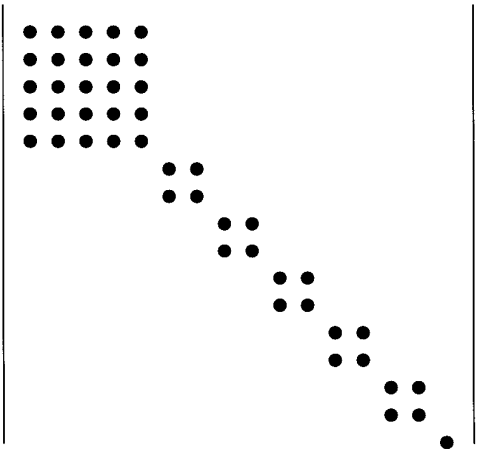

FIG. 3. Schematic of the Delves–Freeman approximate Jacobian. It is identical to the bidiagonal matrix shown in Fig. 2 except for a dense block in the upper left corner, in this case a 5×5 block ($N_D = 3$).

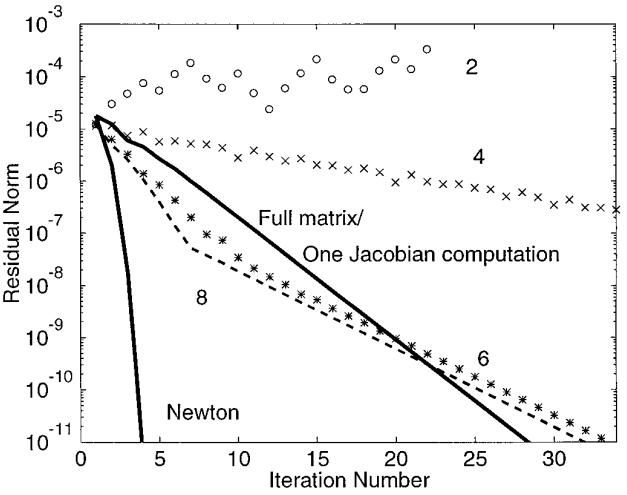

FIG. 4. The decay of the L_∞ norm of the residual vector versus the iteration number. No underrelaxation was used. All cases were initialized with $Q = \varepsilon\ \mathrm{sech}(\varepsilon X)$, which is lowest order perturbation theory. Solid curves: full, dense Jacobian matrix. The lower curve, which passes below the axis after only four iterations, is the standard Newton's method (labelled "Newton"); the upper solid curve (labelled "Full matrix/one Jacobian computed") is the same except that the Jacobian matrix is computed and factored just once into the product of a lower triangular matrix L and an upper triangular matrix U, and these are reused for the remaining iterations. The dashed thin line and the symbols denote Delves–Freeman iterations with a single computation of the Jacobian, identical except for block size. Circles (top of graph, diverges): $N_D = 2$ (3×3 upper left block). Crosses (convergent, but very slowly): $N_D = 4$ (7×7 block). Asterisks: $N_D = 6$ (11×11 block). Dashed line: $N_D = 8$ (15×15 block). The spatial period divided by 2π is $L = 31.503$; $\varepsilon = 1/10$.

approximated Jacobian at each iteration, is shown for comparison; its quadratic convergence appears as the sharp downward ever-increasing slope. This rate of convergence is "digit-doubling" in the sense that the number of correct digits roughly doubles at each iteration. Newton's method needs far fewer iterations than the Delves–Freeman iteration, but is much more expensive.

In contrast, the other cases applied the cheapest option: the Jacobian is just computed once, there is no underrelaxation, and the full Jacobian matrix is approximated by a block-and-bidiagonal matrix with various sized blocks as indicated by the numbers labelling each curve. The bidiagonal approximation (not shown) and also $N_D = 2$, which is a 3×3 block, diverge. However, when $N_D \geqq 6$, which is an upper left 11×11 block, the preconditioned iteration converges geometrically.

The second striking conclusion is that if the Jacobian matrix is computed only once, the rewards for using the full Jacobian matrix are modest indeed: There is only a slight improvement as the size of the upper left block is increased beyond 11×11.

The *size of the block* which is needed for convergence, and the slightly larger size which is optimum for minimizing cost, are *highly problem dependent* and *resolution dependent*. (As evident in Table 2, N must increase as ε decreases; N_D must increase, too, as shown by comparing Figs. 4 and 5, which are the same except for smaller ε in Fig. 5.) However, it is generally true that one obtains fast, geometric

TABLE II

α_{min} versus ε, Third-Order Nonlinear Schroedinger Equation

ε	$\alpha_{\text{numerical}}$	α_{WLC}	L	N
1/10	3.14774E-3	5.09606E-3	81.5093	256
9/100	1.57871E-3	2.12932E-3	131.458	384
8/100	5.96415E-4	7.15318E-4	131.407	384
1/15	9.02336E-5	1.00407E-4	121.340	384
2/35	1.30622E-5	1.40938E-5	201.291	384
1/20	1.86787E-6	1.97831E-6	201.255	384
2/45	2.65467E-7	2.77689E-7	201.226	384
1/25	3.75910E-8	3.89783E-8	219.204	512
2/55	5.31049e-9	5.47127E-9	301.185	640
1/30	7.49039E-10	7.67985E-10	401.170	640
2/63	2.31147e-10	2.36435E-10	380.162	640
1/33	7.13069E-11	7.27898E-11	401.154	640
2/69	2.19918E-11	2.24094E-11	451.147	1024
1/36	6.78101E-12	6.89903E-12	501.141	1024
1/38	1.41215E-12	1.43417E-12	551.134	1024
1/40	2.94006E-13	2.98134E-13	601.127	1024

Note. $\alpha_{\text{WLC}} = 13.1273 \exp(-\pi/(4\varepsilon))$; L = odd integer + $(16/\pi)\ \varepsilon$; N is the number of grid points; the total number of unknowns is $2N$.

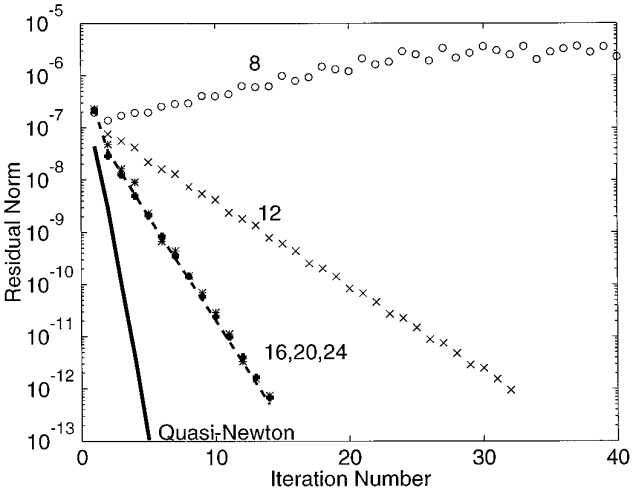

FIG. 5. The decay of the L_∞ norm of the residual vector versus the iteration number. The figure is identical to Fig. 4 except for smaller ε (=1/20). This requires much larger N (=384) both because the spatial period must increase (to accommodate wider core peaks without overlap) and also to accurately compute α, which decreases exponentially with $1/\varepsilon$. Solid curve ("quasi-Newton"): full, dense Jacobian matrix, which is computed and LU-factored just once. The dashed thin line and the symbols denote Delves–Freeman iterations with a single computation of the Jacobian, all identical except for block size. Circles (top of graph, diverges): $N_D = 8$ (15×15 upper left block). Crosses (convergent, but slowly): $N_D = 12$ (23×23 block). Asterisks, plus signs, dashed line ("16, 20, 24"): $N_D = 16$, 20, and 24. (These three curves are almost on top of one another.) The spatial period $P = 1264.52$ ($L = 201.255$).

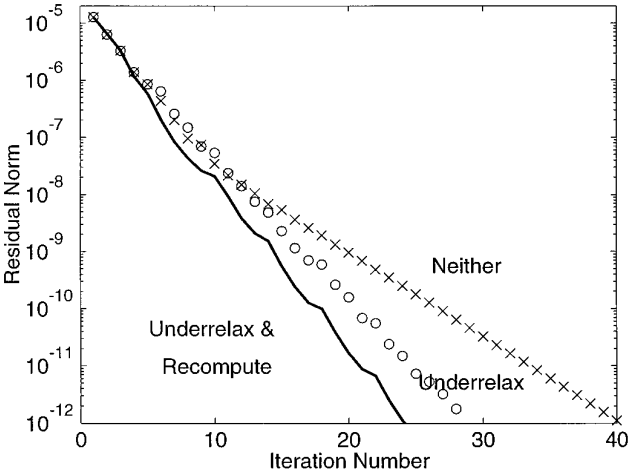

FIG. 6. Three variations on the Delves–Freeman iteration, all with $N_D = 6$ (11×11 upper left block in the approximate Jacobian matrix). Solid curve: The (sparse) Jacobian was recomputed and factored at every iteration, and underrelaxation with τ as small as 1/16 was also used. Circles: The Jacobian was computed just once, but again underrelaxation with τ as small as 1/16 was employed. Crosses: The Jacobian was computed only once and $\tau = 1$ always; that is, the full quasi-Newton correction was applied at every iteration without underrelaxation. The spatial period divided by 2π is $L = 31.503$; $\varepsilon = 1/10$.

convergence from a block size which is small compared to the matrix dimension. The monograph by Delves and Freeman gives an extensive collection of theorems and numerical examples that support this conclusion.

Two choices still remain: Do we recompute the block-and-bidiagonal Jacobian at every iteration or just once? Do we underrelax? (Underrelaxation means multiplying the Newton correction by a constant $\tau < 1$, comparing the residuals for various τ, and choosing whichever gives the smallest residual. We set $\tau = 2^{-j}$, $j = 0, 1, \ldots$ for this search.)

Figure 6 shows that both strategies improve the rate of convergence; unfortunately, both also require many extra operations. Underrelaxation, with but a single computation of the Jacobian, is able to reach the bottom of the graph in 30 iterations, whereas $\tau = 1$ needs 40. Recomputing the Jacobian at every step saves only 5 iterations. If we are blessed with a good initial iterate, as supplied here by lowest-order perturbation theory as the approximation $Q(X) \approx \varepsilon\,\mathrm{sech}(\varepsilon X)$, then underrelaxation and Jacobian recomputation are not worth the bother.

Figure 7a shows that the Jacobian matrix does indeed have small eigenvalues. The V-shaped cluster of eigenvalues pointing downward to the smallest eigenvalue is due to the resonance discussed above: $\exp(-iX/2)$ is an approximate eigenmode of the TNLS equation. We added rows and columns to the Delves–Freeman approximate Jacobian to make no approximation for the basis functions $\cos(jX/L)$ and $\sin(jX/L)$ such that $j \approx j_{\mathrm{res}}$. (Figure 8 illustrates the shape of the sparse matrix—block-plus-bidiagonal plus a band of dense rows and a band of dense columns.) However, this produced only slight improvements in convergence, not enough to justify the added cost. Boyd [37] showed that for a Fourier pseudospectral algorithm

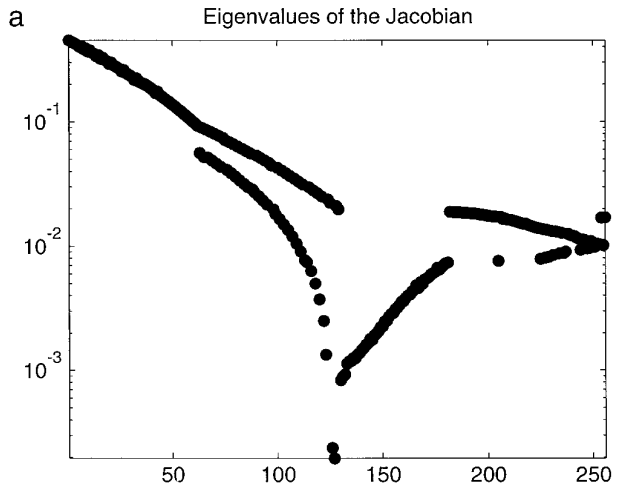

FIG. 7. (a) Absolute values of the eigenvalues of the full (dense) Jacobian matrix. The spatial period divided by 2π is $L = 31.503$; $\varepsilon = 1/10$ and $N = 256$. (b) Top curve: absolute values of the Fourier coefficients of the solution $Q(x)$. Bottom curve: absolute values of the elements of the element-wise product of the 201st row of the full Jacobian matrix with the Fourier coefficients. (This is one of the rows closest to the resonant wavenumber.) (Same case as (a).) (c) Absolute values of the elements of the 201st row of the full Jacobian matrix. (Same case as (a), (b).) The two solid overlapping disks at the top of the graph are the big elements that are part of the bidiagonal matrix. The open circles are the much smaller elements which are not part of the bidiagonal matrix.

in which the Jacobian is approximated by a finite difference matrix, the resonance for the fifth-order Korteweg–deVries equation considerably degrades the rate of convergence. Why does the resonance fail to wreak harm here?

We do not have a full explanation. Delves and Freeman wrote a whole book on the topic and yet never addressed a differential equation with resonances like the third-order nonlinear Schroedinger equation.

What can be said is that in the product of a row of the Jacobian matrix for $j \approx j_{\text{res}}$ with the Fourier coefficients, the two elements which are part of the bidiagonal matrix—and therefore of the Delves–Freeman matrix *without* special treatment for the resonance—dominate the contributions of the other Jacobian elements to this vector-column product (bottom curve, Fig. 7b). Part of the reason is the relatively large size of the Fourier coefficients which multiply the bidiagonal Jacobian elements due to the spike around the resonant wavenumbers visible in the upper curve in Fig. 7b. Another is that the elements of the bidiagonal matrix are huge compared to the off-diagonal elements as shown in Fig. 7c. The resonance simply is not a problem for small ε.

4. HYPERASYMPTOTICS AND THE DELVES-FREEMAN ITERATION

Boyd [25] has described a mixed numerical/analytical algorithm for computing the radiation coefficient α for the TNLS equation and others. It uses concepts from hyperasymptotic perturbation theory, so we shall refer to it simply as the "hyperasymptotic" method [40].

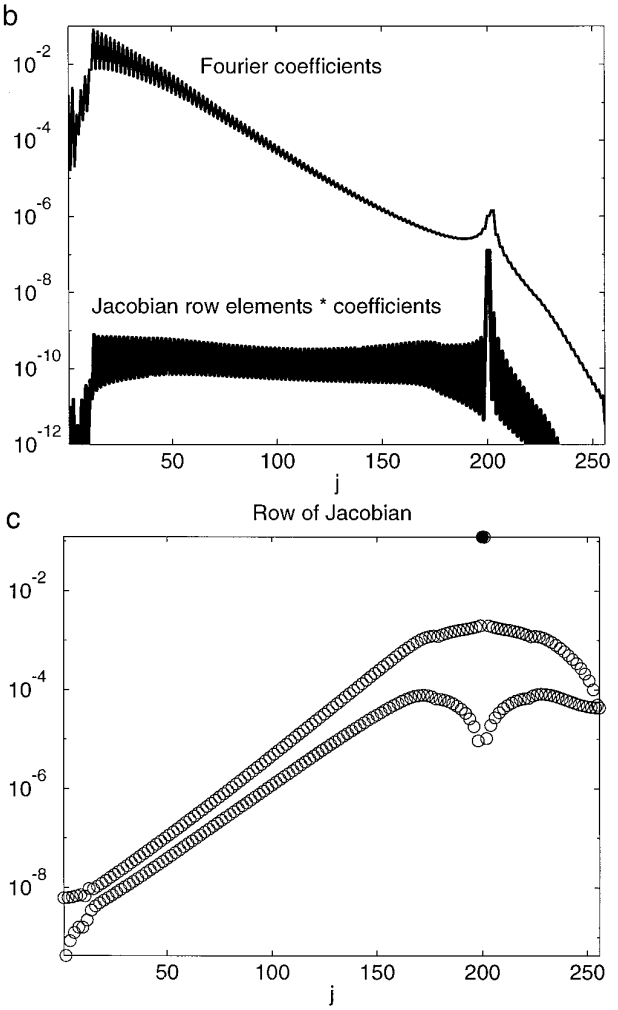

FIG. 7—*Continued*

One part of this scheme, which has no counterpart in the Delves–Freeman method, is to use a high power series expansion in ε to compute a very accurate first approximation. The asymptotic but divergent series is truncated at optimal order $M(\varepsilon)$. This gives a "superasymptotic" approximation whose error is $O(\alpha)$. However, one can show that superasymptotic approximations decay exponentially as $|X| \Rightarrow \infty$ and thus completely miss the far field oscillations.

The second part of the hyperasymptotic algorithm is to apply a single iteration with a diagonal (or bidiagonal) Galerkin matrix and an additional approximation. Employing a bidiagonal approximation to the true Jacobian of the TNLS equation is equivalent to approximating the linearized but variable coefficient operator (2.6) by the *constant coefficient* operator

$$J^{cc}(Q)\,\Delta \equiv \begin{cases} -\frac{1}{2}\varepsilon^2\,\Delta_r - \varepsilon^2\,\Delta_{im,X} + \frac{1}{2}\,\Delta_{r,XX} + \Delta_{im,XXX} \\ -\frac{1}{2}\varepsilon^2\,\Delta_{im} + \varepsilon^2\,\Delta_{r,X} + \frac{1}{2}\Delta_{im,XX} - \Delta_{r,XXX} \end{cases}. \tag{4.1}$$

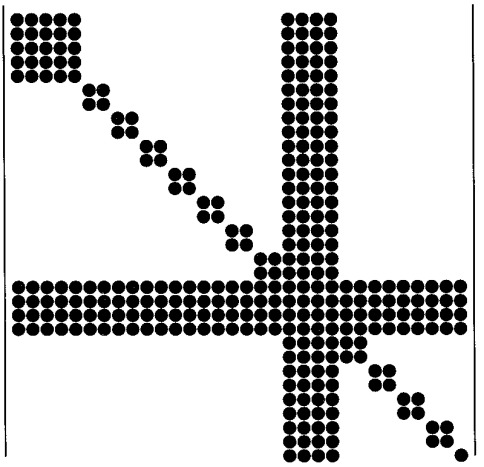

FIG. 8. The circles are the nonzero elements of the Delves–Freeman iteration matrix for a typical case in which full rows and columns have been added to the upper-left-block-plus-bidiagonal matrix illustrated in Fig. 3. The resonant wavenumber j_{res} is halfway between two integers whenever the spatial period P is chosen to give minimum amplitude α_{min} to the oscillatory wings. Thus, the simplest modification for resonance is shown, which is to give full rows and columns to the four basis functions $\{\cos([j_{\text{res}} \pm 1/2]X/L), \sin([j_{\text{res}} \pm 1/2]X/L)\}$.

Although it is not possible to completely solve the linear constant coefficient differential equation (4.1), there is an analytic approximation to its *asymptotic,* large $|X|$ behavior [25] which is sufficient to give the radiation coefficient α. The replacement of the true Jacobian by the constant coefficient differential operator (4.1) limits the accuracy of the method to the determination of ν_0 and ν_1 [25]. Thus, to compute the $O(\varepsilon^2)$ factor in α, we need something better, as done here numerically.

Still, there is a close similarity between the hyperasymptotic scheme of [25] and the Delves–Freeman iteration in the sense that both approximate the Jacobian operator by something simpler. Indeed, the hyperasymptotic method uses a bidiagonal matrix as the approximation. But how can this succeed when we have already seen that the Delves–Freeman iteration *diverges* unless we include at least a small dense block of elements?

The answer is that the upper left-hand block of the Delves–Freeman iteration matrix couples only low-order basis functions. However, the residual of the optimally truncated perturbation theory has negligible amplitude at low wavenumbers (small j): the perturbation theory has purged it [25, 39]. The treatment of these modes in the upper left corner of the Galerkin matrix for the Jacobian operator is *irrelevant* because these modes have no amplitude in the perturbative residual. The residual of the superasymptotic approximation is peaked at $k = -1/2$. For this wavenumber, the bidiagonal matrix is quite sufficient.

Boyd [25] made the claim that one could repeat the bidiagonal iteration indefinitely to obtain a geometrically convergent numerical method. This claim is not true for the TNLS equation! The bidiagonal matrix is successful only in the spirit of an asymptotic but divergent procedure: One iteration is good, but many iterations will fail because error will gradually build up in the low wavenumbers.

By adding an upper left block, we have a more difficult linear algebra problem to solve at each iteration, and it must be solved numerically rather than analytically as in [25]. There are two rewards. First, if the block is sufficiently large, the iteration converges! Second, it is not necessary to use *high-order* perturbation theory to initialize the iteration. Instead, all calculations shown here were initialized with the lowest-order perturbative approximation, $Q(X) = \varepsilon\ \mathrm{sech}(\varepsilon X)$.

5. NUMERICAL RESULTS: NANOPTERONS AND NANOPTEROIDAL WAVES

Figure 9 is one visualization of the exponential dependence of the radiation coefficient α versus ε. Figure 9a is a surface plot that illustrates how the shape of the nanopteron changes as ε doubles: from no visible oscillations at $\varepsilon = 0.075$ to very large oscillatory wings at $\varepsilon = 0.15$. Figure 9b compares the shape of the nanopteron at the extremes of the surface plot.

Figure 10 is a second visualization of the same thing: a plot of α versus $1/\varepsilon$. On this semilogarithmic graph, the prediction of the matched asymptotics formula of Wai *et al.* [12] is that α should asymptote to a straight line as $1/\varepsilon$ increases with slope $-\pi/4$. Their formula

$$\alpha_{\mathrm{WLC}}(\varepsilon) \sim 13.1273 \exp\left(-\frac{\pi}{4\varepsilon}\right), \qquad \varepsilon \to 0 \tag{5.1}$$

is a good approximation for small ε as shown by the dashed curve in Fig. 10. (Note, however, that their $\nu_0 \approx 13.24$ and Grimshaw's $\nu_0 \approx 13.48$ [26] have been replaced by the highly accurate value from [25].) Table 2 gives the numerical results. The spatial period P (or equivalently, $L = P/(2\pi)$) was chosen to give the minimum radiation coefficient for a given ε, $\alpha_{\min}(\varepsilon)$, using the formula derived in Appendix B.

To calculate higher-order corrections to (5.1), we applied least squares polynomial fitting. Define $\nu(\varepsilon)$ to be the ratio of the numerically computed radiation coefficient to $\alpha_{\mathrm{WLC}}(\varepsilon)$, that is,

$$\nu(\varepsilon) \equiv \frac{\alpha_{\min}(\varepsilon)}{13.1273 \exp\left(-\dfrac{\pi}{4\varepsilon}\right)}. \tag{5.2}$$

The linear and quadratic coefficients in $\nu(\varepsilon)$ are then

$$\nu_1 = \lim_{\varepsilon \to 0} \left\{ \frac{\nu(\varepsilon) - 1}{\varepsilon} \right\}, \qquad \nu_2 = \lim_{\varepsilon \to 0} \left\{ \frac{\nu(\varepsilon) - 1 - \nu_1 \varepsilon}{\varepsilon^2} \right\}. \tag{5.3}$$

We compute polynomial fits to each of the quantities in braces in (5.3) and then extrapolate to $\varepsilon = 0$. The fits are by polynomials of various degrees on the interval $\varepsilon \in [1/40, \varepsilon_0]$ where ε_0 is also varied.

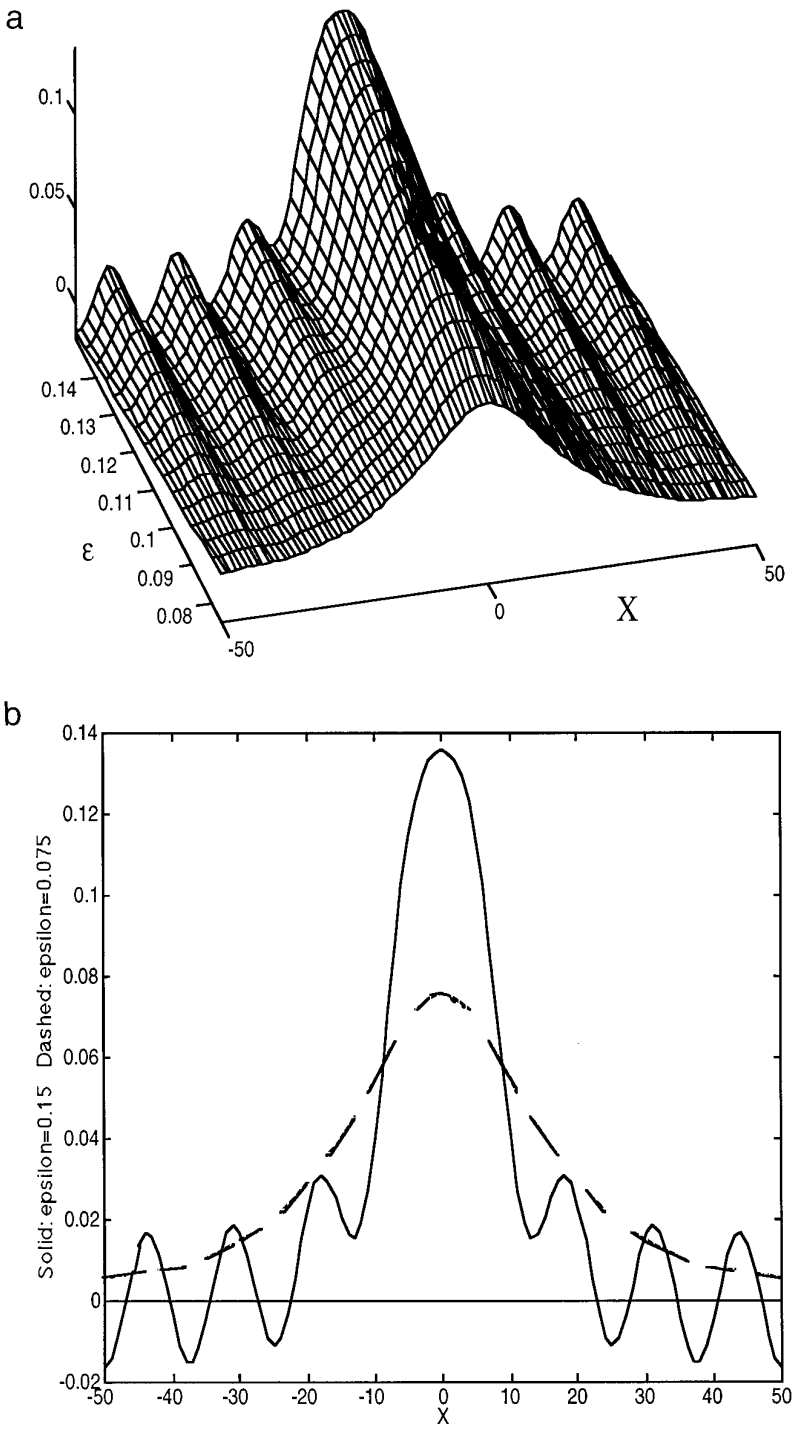

FIG. 9. (a) Real part of $Q(X; \varepsilon)$ for the nanopteroidal wave with $\varepsilon \in [0.075, 0.15]$ with spatial period $P = 100$. (Because the spatial period is fixed, the wings are not the smallest far field oscillations which are possible for a given ε.) (b) Same as (a), but showing the extremes. Solid: $\varepsilon = 0.15$. Dashed: $\varepsilon = 0.075$.

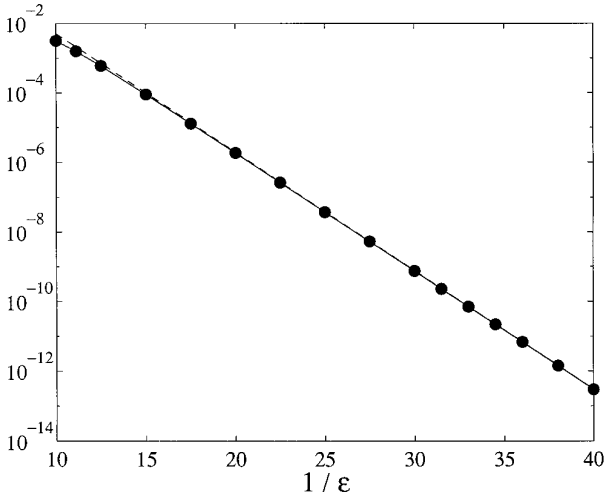

FIG. 10. Solid-and-circles: Numerical computations of α. Dashed-and-asterisks: $\alpha_{\rm WCL} \equiv 13.24 \exp(-\pi/[4\varepsilon])$, which is the matched asymptotics prediction of Wai *et al.* [12]. (The two curves are almost indistinguishable except for a slight gap on the left.) The numerical computations were actually of nanopteroidal waves with L = odd integer + $(16/\pi)\varepsilon$ where the spatial period is $P = 2\pi L$; the ε factor in L ensured that minimum α was computed for each ε. P is sufficiently large so that the overlap between adjacent core peaks is very small in comparison to α so that these results apply to nanopterons, too.

In single precision, it is not possible to compute α reliably for smaller ε because $\alpha(1/40) = 2.9 \times 10^{-13}$; the wings are already smaller than the core peaks by a factor of more than 2 billion! For $\varepsilon < 1/40$, the wings are lost in the roundoff error of the vastly larger core.

We must anticipate that the fit will be poor when ε_0 is close to 1/10 for all degrees of the fitting polynomial since the larger values of ε will be contaminated by $\nu_3\,\varepsilon^3$ and higher corrections. Since extrapolation of high degree interpolating polynomials is notoriously ill-conditioned, we expect that errors will also be large when a fourth degree polynomial is fitted to just five points, for example, as happens when the upper limit of the fitted range ε_0 is too close to the lower range, $\varepsilon = 1/40$. Thus, the most reliable estimates for ν_1 and ν_2 are likely to come when (i) ε_0 is in the intermediate range and (ii) the degree of the fitting polynomial is moderate.

Figures 11 and 12 confirm these expectations. The convergence of the linear, quadratic, and cubic fits for ε_0 between [0.04 and 0.06] suggests that $|\nu_1| < 1/100$. Because the quadratic coefficient is much larger—roughly -22—we conjecture that the exact value of the linear coefficient is

$$\nu_1 = 0. \tag{5.4}$$

Of course, we cannot prove such a conjecture from any amount of numerical calculations, but rather merely put tighter and tighter bounds around some number as our resolution improves. However, it seems very unlikely that the true value of ν_1 would be nonzero and yet more than 2000 times smaller than the quadratic coefficient.

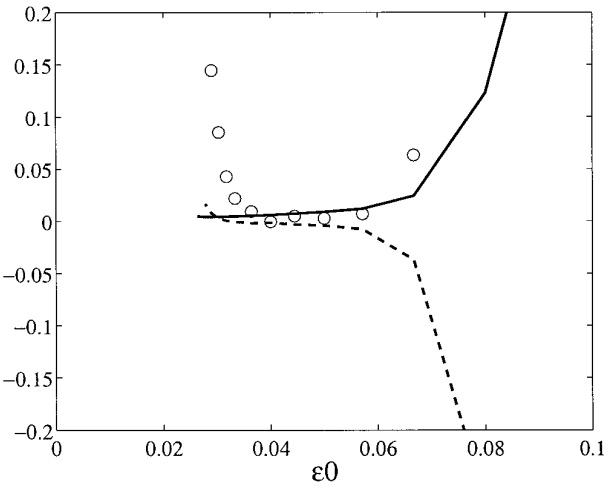

FIG. 11. Estimates of ν_1 via polynomial fitting of values in the range [1/40, ε_0] where ε_0 is the horizontal axis of the graph. Solid line: linear polynomial fit. Dashed line: quadratic polynomial. Circles: third degree polynomial.

In estimating ν_2, we therefore set $\nu_1 = 0$ in the right half of (5.3). Figure 6 shows the resulting fits:

$$\nu_2 \approx -22.0 \, to \, -22.2. \tag{5.5}$$

Figure 13 compares the quadratic approximation, $\nu(\varepsilon) \approx 1 - 22.0\ \varepsilon^2$ with the Delves–Freeman results. We have rounded off our estimate (5.5) to the nearest integer because of the uncertainty in the digit after the decimal place.

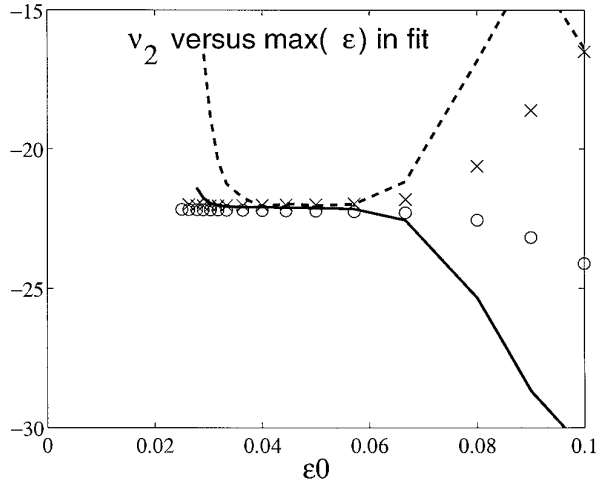

FIG. 12. Estimates of ν_2 via polynomial fitting of values in the range [1/40, ε_0] where ε_0 is the horizontal axis. x's: constant (zero degree) polynomial fit. Solid line: linear polynomial fit. Dashed line: quadratic polynomial. Circles: third degree polynomial.

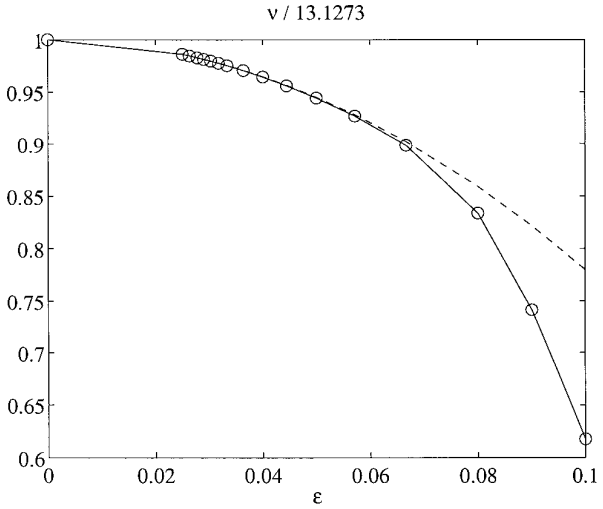

FIG. 13. $\nu(\varepsilon)$ divided by 13.1273 is shown as the solid curve with circles where the symbols mark the data points (plus the limit at $\varepsilon = 0$). The dashed curve (without symbols) is the fit: $\nu \approx 13.1273\ (1 - 22\ \varepsilon^2)$.

A higher-than-quadratic approximation is clearly needed for $\varepsilon > 0.06$, but for smaller values of ε, the second degree polynomial gives a very good approximation.

Grimshaw and Joshi [36] have successfully applied matched asymptotics expansions to compute ν_1 and ν_2 for the fifth-order Korteweg–deVries (FKdV) equation. However, the analysis is difficult. Boyd [37] has numerically confirmed ν_1, but there is a discrepancy for ν_2.

No such perturbative extension has yet been done for the TNLS equation, so ν_1 and ν_2 are calculated for the first time here. However, our TNLS results should be sufficiently accurate to guide and to check higher "beyond-all-orders" asymptotics.

6. BIONS

Akylas and Kung [1] and Klauder *et al.* [18] computed TNLS "bions." These are bound states of solitary waves which consist of two ordinary solitary waves bound together by the $O(\alpha)$ oscillations between the two cores (Fig. 14). They also observed that for *discrete* parameter values, the wing oscillations of the two solitons *cancelled exactly* in the far field so that the bion is a *classical* solitary wave. If one traces a particular branch of the bion by varying ε, the amplitude-and-width parameter, then the wings vanish for *discrete* values of ε. (The oscillations *between* the cores do not disappear because these between-the-core oscillations are the glue that binds the two peaks together.)

In a similar spirit, Branis *et al.* [21] and Branis and Martin [22] calculated radiation-free envelope solitary waves of the Maxwell–Bloch equations. Vanden-Broeck [34, 35] did the same for water waves. Like the TNLS bions, the Maxwell–Bloch and water wave solitons have $\alpha = 0$ only for *discrete* parameter values. However, their solutions are not bions, but rather ordinary solitary waves with only a single core

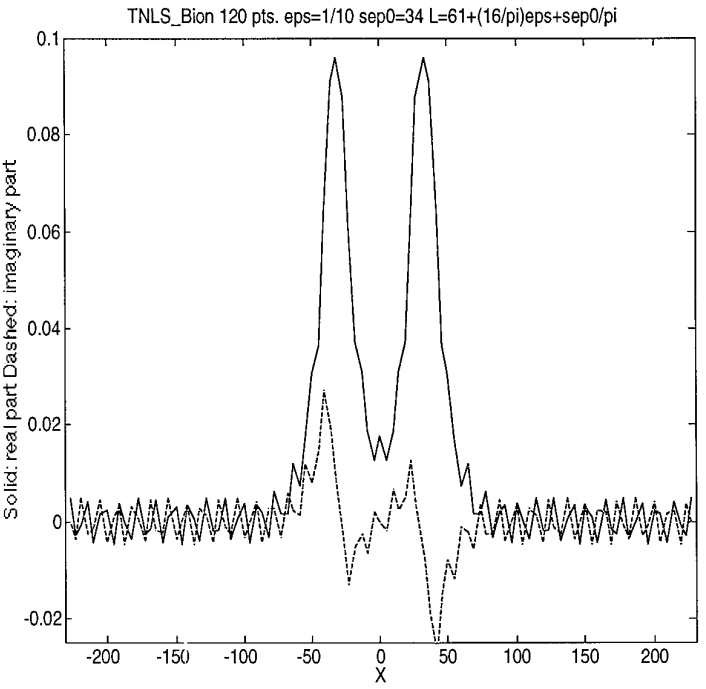

FIG. 14. A TNLS bion with $\varepsilon = 1/10$; the first guess was two ordinary solitons separated by 68. This bion was approximated by computing a bion-like nanopteroidal wave on a large spatial period P. The spatial period is $P = 2\pi L$ where $L = 61 + (16/\pi)\varepsilon + 34/\pi$, which implies the minimum far field oscillations for this amplitude.

peak or trough. The cancellation of one soliton far field by another is clearly not necessary for classical coherent structures to coexist with weakly nonlocal solitary waves.

Bions are interesting because Klauder *et al.* [18] observe that for fiber optics communications, it might be desirable to send pulses in the form of radiation-free bions to minimize radiation losses. It is unclear, however, whether laser diodes can efficiently generate such bions with widths tuned to the precise values for which $\alpha = 0$. Furthermore, the binding between the two peaks is the shared, oscillatory wing between them and is therefore weak. Still, communication-by-bion *is* an intriguing possibility. Figure 14 shows that the Fourier–Galerkin method works just as well for bions as for ordinary nanopterons, which have but a single peak.

7. SUMMARY

The Delves–Freeman iteration works well for the third-order nonlinear Schroedinger equation. It makes it possible to calculate the amplitude α of the oscillatory wings that radiate from the large core of the nanopteron to spectral accuracy at low cost. The great savings arise because it is not necessary to compute or store the full Fourier–Galerkin matrix. Instead, it is sufficient to compute a dense upper

left-hand block. In our experiments, this block was always less than 10% of the size of the Galerkin matrix as a whole, representing a cost savings of $O(100)$ in both computing and storing the elements and in performing the LU factorization of the matrix.

Somewhat to our surprise [37], no special treatment was needed because of the resonance which creates the oscillatory wings of the solitary wave and simultaneously forces some eigenvalues of the Jacobian matrix to be small. The Delves–Freeman iteration is quite robust and stable.

Although our problem has only a single spatial coordinate, the method generalizes well to higher dimensions if the unknowns are ordered so that low wavenumbers in both x and y appear as the first few rows and columns of the Galerkin matrix. (This reordering can be done explicitly, but a good sparse matrix solver may *implicitly* accomplish the same thing.) One can then approximate the full Galerkin matrix by a block-plus-banded matrix.

Despite all these good qualities and the publication of the 1981 monograph by Delves and Freeman [28], their method has fallen into disuse. We know of no application more recent than the early 1980s except for a simple example in the author's own book [29].

This article has inflicted a heavy dose of the theory of weakly nonlocal solitary waves on the reader and includes some modest additions to the extensive existing theory of the TNLS equation. The only apology we can make to readers primarily interested in numerical methods, and not this particular phenomenon, is to note that numerical computations are sound only when built on a foundation of physical understanding.

Eugene Wigner once said, "It is nice to know that the computer understands the problem. But I would like to understand it, too." His joke is a witty claim that one can solve a problem numerically with much less thought than to solve it analytically. This is sometimes true, but only sometimes. Often, theoreticians can happily live with gaps in understanding which are intolerable to the machine. Our two appendices are a counterclaim to Wigner: To solve the TNLS equation numerically, one must *really* understand it. And this is true of many other scientific computations as well.

APPENDIX A: THEORY OF THE TNLS EQUATION

The general third-order nonlinear Schroedinger equation is

$$iA_t + \frac{1}{2}w''A_{\zeta\zeta} + \nu|A|^2A - i\beta A_{\zeta\zeta\zeta} = 0, \tag{A.1}$$

where $A(X, t)$ is the envelope of a nonlinear wave packet:

$$u(x, t) = A(x - c_g t, t)\exp(ik[x - c_p t]) + \textit{complex conjugate.} \tag{A.2}$$

The TNLS equation describes the evolution of the envelope only and its solutions are generally *complex-valued.* It is written in a coordinate system that moves at

the *linear* group velocity of a wave with wavenumber equal to that of the carrier wave of the packet, i. e.,

$$\zeta \equiv x - c_g(k)t. \tag{A.3}$$

The method of multiple scales, a singular perturbation scheme, shows that many species of partial differential equations have solutions of the form of (A.2) in the limit of small amplitude (Table 1).

The time-dependent TNLS equation can be reduced to our nonlinear boundary value problem (1.1) in four stages. First, (A.1) can be reduced by simple rescalings to an equation with coefficients all of absolute value one or one-half.

THEOREM A.1. *If* $U(X, T; w'', \nu, \beta)$ *solves*

$$iU_T + \tfrac{1}{2}w''U_{ZZ} + \nu|U|^2U - i\beta U_{ZZZ} = 0, \tag{A.4}$$

where w'' *is the second derivative with respect to wavenumber* k *of the dispersion relation,* $w(k)$, *and* $\nu(k)$ *is the "Landau constant," then*

$$U(Z, T) = \rho A\left(\frac{Z}{L}, \frac{T}{M}\right), \tag{A.5}$$

where $A(\zeta, t)$ *satisfies*

$$iA_t + \tfrac{1}{2}A_{\zeta\zeta} + |A|^2A - iA_{\zeta\zeta\zeta} = 0 \tag{A.6}$$

with

$$L = \frac{\beta}{w''}, \qquad M = \frac{\beta^2}{(w'')^3}, \qquad \rho = \frac{(w'')^{3/2}}{\nu^{1/2}\beta} \tag{A.7}$$

Proof. Substitution of (A.5) and (A.7) into (A.4).

The second step is to note that the general soliton contains a multiplicative factor of $\exp(-i\kappa x)$ which effectively shifts the wavenumber k of the carrier wave by κ without otherwise altering the dynamics. In studying soliton-soliton collisions, the extra degree of freedom represented by κ is useful. For a *single* solitary wave, however, the wavenumber shift κ is not useful because we can always redefine the wavenumber k of the carrier wave so as to set $\kappa = 0$, as is done throughout this paper.

The third simplification is to observe that the relationships that connect the carrier frequency shift ω and group velocity shift γ to ε are terminating ε-perturbation series so that, as already done in (1.1), we can simply replace ω by $\varepsilon^2/2$ and γ by $-\varepsilon^2$. Grimshaw [26] has explained why these relationships are exact. In the "far field" where the core has decayed to the wing oscillations, the nonlinear term in the TNLS equation can be neglected. Grimshaw's asymptotic analysis shows that the core can decay as $\exp(-\varepsilon|x|)$ if and only if the series for ω and γ are terminating series. (Corrections "beyond all orders" in ε cannot be ruled out, however.)

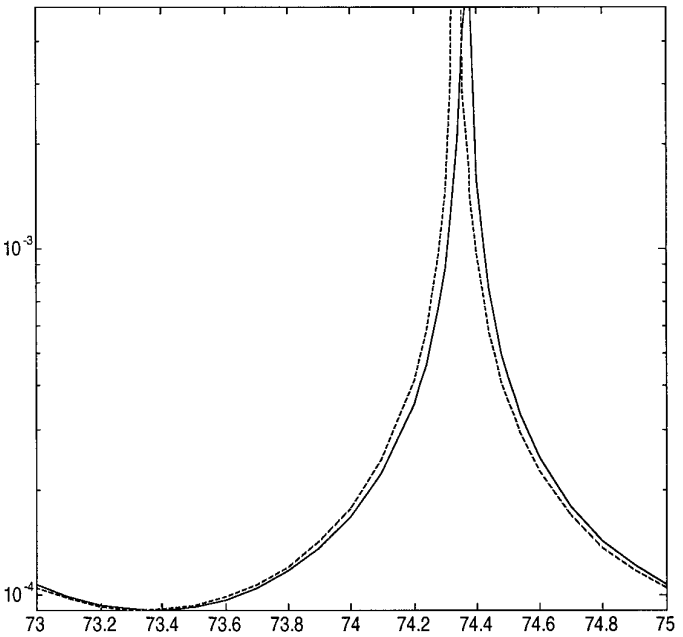

FIG. 15. $|\alpha|$ versus L for $\varepsilon = 1/15$. Solid: numerical computations of α with 64 grid points. Dashed: theoretical prediction, Eqs. (B.8)–(B.9).

The fourth simplification is to assume that the real part of the nanopteron is symmetric with respect to $X = 0$ and that the imaginary part is antisymmetric. Grimshaw [26] proves that the wing oscillations must have equal amplitude, but this does not rule out asymmetric core structures. Bound states of multiple cores in which the cores are of slightly different sizes are a possibility. However, previous work has left no doubt that there are solutions that satisfy these symmetry restrictions.

APPENDIX B: EIGENFUNCTIONS

For reasons too complicated to explain here (but see the author's monograph [39]), the most interesting nanopterons are those of minimal far field oscillations. (One can show that a localized initial condition will spontaneously evolve to a state that can be approximated by such a minimum-α nanopteron, or a sum of such nanopterons, behind the ever-widening wave front.) These nanopterons with $\alpha = \alpha_{\min}$ can be approximated by nanopteroidal waves, that is, by solutions of the same differential equation but with boundary conditions of spatial periodicity with period P. Figure 15 shows the computed amplitude of α versus the period divided by 2π. Clearly, the amplitude of the wings can vary wildly with P. What values of P give $\alpha = \alpha_{\min}$? We can answer this question, at least approximately, by analyzing the eigenfunctions of the linearized TNLS equation as done in the rest of this appendix.

The Jacobian operator $J(Q)$, defined by (2.4), has a zero eigenvalue when $Q = Q_{\text{sol}}(X)$, the nanopteron. In other words, there are nontrivial functions $e_j(X)$ such that

$$J(Q_{\rm sol})e_j = 0, \qquad \forall X. \tag{B.1}$$

Because the TNLS equation is translationally invariant, it must have the X-derivative of the soliton as one such eigenfunction. Since differentiation changes symmetric functions into antisymmetric and vice versa, the parity of this translational eigenfunction $e_{\rm trans}(X) = Q_{{\rm sol},X}$ is *opposite* that of the nanopteron or nanopteroidal wave. The exploitation of symmetry (so that the real part of $Q_{\rm sol}$ is approximated by a cosine series) automatically filters this mode. Consequently, the Jacobian matrix is nonsingular and the translational eigenfunction has no numerical significance.

It also has no physical significance in the sense that the new solution generated by adding $\delta\ e_{\rm trans}$ to a solution $Q_{\rm sol}(X)$ merely gives the same solution with a translation, that is,

$$Q_{\rm sol}(X) + \delta e_{\rm trans} \approx Q_{\rm sol}(X + \delta). \tag{B.2}$$

The other eigenfunction of zero eigenvalue *exists only on the infinite spatial interval*, but it has profound implications for the spatially periodic problem, too. It arises because the function

$$Q(X) = \exp(-iX/2) \tag{B.3}$$

solves the TNLS equation when the nonlinear term is neglected. (There are two other homogeneous solutions to the constant coefficient, third-order equation that approximates the TNLS equation in the ''far field,'' but these are unbounded as $|X| \Rightarrow \infty$.) Because the cubically nonlinear term is $O(\varepsilon^2)$ for the nanopteron, it follows that $\exp(-iX/2)$ is also an approximate eigenfunction of $J(Q_{\rm sol})$ with an error of $O(\varepsilon^2)$.

This much was known to Grimshaw [26] and is implicit in the work of other previous workers. To compute $\alpha_{\rm min}$ up to and including the $O(\varepsilon^2)$ corrections, we need a more accurate $O(\varepsilon)$ approximation to the eigenfunctions. This in turn will give us an equally accurate formula for the spatial period that gives the minimum α for a given ε.

The eigenfunction can be approximated more accurately by generalizing the WKB method to give

$$e_2(X;\varepsilon) \sim \exp\left(-i\frac{1}{2}X + 8i\varepsilon\tanh(\varepsilon X)\right). \tag{B.4}$$

Without loss of generality, the nanopteron can be written in the form

$$Q(X) = A(X)\exp(i\Xi(X)), \tag{B.5}$$

where $A(X)$ asymptotes to a constant (not necessarily the same constant) for $X \Rightarrow \pm\infty$ and Ξ asymptotes to a linear function of X. By examining the various cases, one can show that the real part of $Q(X)$ is symmetric with respect to the origin and the imaginary part is antisymmetric if and only if (i) $\Xi(X)$ is antisymmetric with respect to X, (ii) $\mathrm{Re}(A)$ is symmetric, and (iii) $\mathrm{Im}(A)$ is antisymmetric. This

implies that while we may add $\delta e_2(X;\varepsilon)$ for small but arbitrary δ to a nanopteron to generate a new function that is also an approximate solution in the sense of an error no larger than $O(\delta^2)$, the multiplier δ must be *real* to preserve the symmetries. One may further show that if an arbitrary real multiple of the eigenfunction defined by (B.4) is added to a nanopteron, the amplitude of $Q(X)$ in the far field, i.e., $|\alpha|$, is minimized when δ is such that α is pure imaginary.

Let $\alpha_{\min}(\varepsilon)$ be the minimum amplitude of the far field oscillations for a given ε, minimized over the eigenfunction multiplier δ. (For nanopteroidal waves, apply the same definition but minimized over the period P.) The general far field of the nanopteron is then

$$Q(X) \sim \begin{cases} (\delta + i\alpha_{\min}) \exp\left(-i\frac{1}{2}X + 8i\varepsilon\right), & X \to \infty \\ (\delta - i\alpha_{\min}) \exp\left(-i\frac{1}{2}X - 8i\varepsilon\right), & X \to -\infty \end{cases}. \tag{B.6}$$

If we define the radiation coefficient α and far field phase Φ via

$$\alpha \equiv \alpha_{\min} - i\delta, \qquad \Phi \equiv \arg(\alpha), \tag{B.7}$$

elementary trigonometric identities show

$$|\alpha(\varepsilon;\Phi)| = \frac{\alpha_{\min}(\varepsilon)}{\cos(\Phi)}. \tag{B.8}$$

Equation (B.8) predicts resonances—unbounded amplitude of the far field oscillations—when the far field phase factor Φ is a root of the cosine. At the opposite extreme, the wings are minimized when $\Phi = \pi m$ where m is any integer; in this case, $\delta = 0$ (i. e., the amplitude of the eigenfunction e_2 is zero) and $\alpha = \pm\alpha_{\min}$.

For the nanopteron, that is, on the domain $X \in [-\infty, \infty]$, the phase factor Φ is simply an extra free parameter. When $Q(X)$ is required to be spatially periodic with period P, however, the phase difference between the two asymptotic limits in (B.9) at $X = \pm P/2$ must be a multiple of 2π, or else Q will be discontinuous:

$$\frac{P}{2} - 16\varepsilon - 2\phi - \pi = 2\pi m, \qquad m = \text{integer}. \tag{B.9}$$

(This assumes that $P \gg 1/\varepsilon$, which is necessary so that the nanopteroidal wave may be approximated by the nanopteron on $X \in [-P/2, P/2]$.) For fixed period, this can be solved for the far field phase Φ and thence for α. Alternatively, if we define L via

$$P = 2\pi L \tag{B.10}$$

we can solve for those values of L for which we obtain resonance or a minimum far field:

$$L_{\text{resonance}} = 2m + \frac{16}{\pi}\varepsilon, \qquad m = \text{integer} \tag{B.11}$$

$$L_{\min} = 2m + 1 + \frac{16}{\pi}\varepsilon, \qquad m = \text{integer}. \tag{B.12}$$

We expect a pole in $\alpha(L)$ wherever L is an odd integer and a minima where L is an even integer, both slightly shifted by $(16/\pi)\varepsilon$.

Figure 15 shows α versus L (= the period $P/2\pi$). The minima at $L = 73.364$ is close to the prediction of Eq. (3.16), L_{pred}=73.3395; L is shifted from the odd integer by about 6.7% too little by the analytical approximation, $(16/\pi)\varepsilon$. Similarly, the predicted and theoretical peaks are very close. The error increases as $\alpha \Rightarrow \infty$ because the nanopteron is no longer "weakly" nonlocal when the wings are large, and the linear far field analysis is no longer very accurate.

It seems likely on the basis of dynamical systems theory that sufficiently close to a resonance, TNLS solutions are chaotic and steadily moving periodic solutions do not exist except perhaps at discrete values of L within the chaotic region.

The Jacobian operator on the spatially periodic domain does not have an eigenfunction of zero eigenvalue. However, the Fourier components with $j = L/2 \pm 1/2$ are sufficiently close to the infinite interval eigenfunction (B.4) so as to have *small* eigenvalues. When the spatial period is chosen to minimize α, the resonant wavenumber $K = -1/2$ ($\Leftrightarrow j = L/2$) corresponds to a Fourier degree j which is halfway between two integers so there is a near-resonance, but no exact resonance. The two near-resonant Fourier coefficients are given special treatment as reported in Section 3, but the small eigenvalues were not so small as to make this special treatment really necessary, as explained above.

Eq. (B.16), which is correct up to and including $O(\varepsilon)$, makes it possible to compute the proportionality constant in front of α up to and including $O(\varepsilon^2)$. (The accuracy limit is $O(\varepsilon^2)$ instead of merely $O(\varepsilon)$ because close to the value of L which gives $\alpha_{\min}$, the dependence of α on L is flat [zero slope at the minimum itself]. Thus, an $O(\varepsilon^2)$ error in L contributes to $\alpha_{\min}$ only at $O(\varepsilon^3)$.)

ACKNOWLEDGMENTS

This work was supported by the NSF through Grants DMS8716766, ECS9012263, OCE9119459, and OCE9521133 and by the Department of Energy through Grant KC070101. I thank Roger Grimshaw, T. R. Akylas, and David Calvo for sending me copies of their work in advance of publication.

REFERENCES

1. T. R. Aklyas and T.-J. Kung, On nonlinear wave envelopes of permanent form near a caustic, *J. Fluid Mech.* **214,** 489 (1990).
2. E. D. Brown, S. Buchsbaum, R. E. Hall, J. P. Penhune, K. F. Schmitt, K. M. Watson, and D. C. Wyatt, Observations of a nonlinear solitary wavepacket in the Kelvin wave of a ship, *J. Fluid Mech.* **204,** 263 (1989).
3. A. M. Glass, Fiber optics, *Phys. Today* **46,** 34 (1993).
4. A. Hasegawa, *Optical Fibers* (Springer-Verlag, New York, 1989).

5. P. D. Drummond, R. M. Shelby, S. R. Friberg, and Y. Yamamoto, Quantum solitons in optical fibres, *Nature* **365,** 307 (1993).
6. E. Desurvire, The Golden Age of optical fiber amplifiers, *Phys. Today* **47,** 20 (1994).
7. J. P. Boyd, New directions in solitons and nonlinear periodic waves: Polycnoidal waves, imbricated solitons, weakly non-local solitary waves and numerical boundary value algorithms, in *Advances in Applied Mechanics,* edited by T.-Y. Wu and J. W. Hutchinson (Academic Press, New York, 1989) Vol. 27, p. 1.
8. J. P. Boyd, Weakly non-local solitary waves, in *Nonlinear Topics in Ocean Physics,* edited by A. R. Osborne and L. Bergamasco (North-Holland, Amsterdam, 1991), p. 527.
9. H. Segur, S. Tanveer, and H. Levine (Eds.), Asymptotics beyond All Orders (Plenum, New York, 1991).
10. J. P. Boyd, Weakly non-local solitons for capillary-gravity waves: Fifth-degree Korteweg–deVries equation, *Physica D* **48,** 129 (1991).
11. P. K. A. Wai, C. R. Menyuk, Y. C. Lee, and H. H. Chen, Nonlinear pulse propagation in the neighborhood of the zero-dispersion wavelength of monomode optical fibers, *Opt. Lett.* **11,** 464 (1986).
12. P. K. A. Wai, H. H. Chen, and Y. C. Lee, Radiation by "solitons" at the zero group-dispersion wavelength of single-mode optical fibers, *Phys. Rev. A* **41,** 426 (1990).
13. H. H. Kuehl and C.-Y. Zhang, Effects of higher-order dispersion on envelope solitons, *Phys. Fluids B* **2,** 889 (1990).
14. Y. S. Kivshar, Nonlinear dynamics near the zero dispersion point in optical fibers, *Phys. Rev. A* **43,** 1677 (1991).
15. J. N. Elgin, Soliton propagation in an optical fiber with 3rd-order dispersion, *Opt. Lett.* **17,** 1409 (1992).
16. J. N. Elgin, Perturbations of optical solitons, *Phys. Rev. A* **47,** 4331 (1993).
17. B. A. Malomed, Bound states of envelope solitons, *Phys. Rev. E* **47,** 2874 (1993).
18. M. Klauder, E. W. Laedke, K. H. Spatschek, and S. K. Turitsyn, Pulse propagation in optical fibers near the zero dispersion point, *Phys. Rev. E,* **47,** R3844 (1993).
19. V. I. Karpman, Radiation by solitons due to higher-order dispersion, *Phys. Rev. E.* **47,** 2073 (1993).
20. M. Oikawa, Effect of the third-order dispersion on the Nonlinear Schroedinger equation, *J. Phys. Soc. Japan* **62,** 2324 (1993).
21. S. V. Branis, O. Martin, and J. L. Birman, Self-induced transparency selects discrete velocities for solitary-wave solutions, *Phys. Rev. A* **43,** 1549 (1991).
22. O. Martin and S. V. Branis, Solitary waves in self-induced transparency, in *Asymptotics beyond All Orders,* edited by H. Segur, S. Tanveer, and H. Levine (Plenum, New York, 1991), p. 327.
23. Y. S. Kivshar and S. K. Turitsyn, Lattice solitons on a standing carrier wave, *Phys. Lett. A* **171,** 344 (1992).
24. J. P. Boyd, Weakly nonlocal envelope solitary waves: Numerical calculations for the Klein-Gordon (ϕ^4) equation, *Wave Motion* **21,** 311 (1995).
25. J. P. Boyd, A hyperasymptotic perturbative method for computing the radiation coefficient for weakly nonlocal solitary waves, *J. Comput. Phys.* **120,** 15 (1995).
26. R. Grimshaw, Weakly nonlocal solitary waves in a singularly perturbed nonlinear Schroedinger equation, *Stud. Appl. Math.* **94,** 257 (1995).
27. D. C. Calvo and T. R. Akylas, On the formation of bound states by interacting nonlocal solitary waves, *Physica D* **101,** 297 (1997).
28. L. M. Delves and T. N. Freeman, *Analysis of Global Expansion Methods: Weakly Asymptotically Diagonal Systems* (Academic Press, New York, 1981).
29. J. P. Boyd, *Chebyshev and Fourier Spectral Methods* (Springer-Verlag, Heidelberg, 1989).
30. Y. Morchoisne, Resolution of Navier–Stokes equations by a space-time pseudospectral method, *Rech. Aerosp.* **1979–5,** 293 (1979).

31. S. A. Orszag, Spectral methods for problems in complex geometries, *J. Comput. Phys.* **37,** 70 (1980).
32. M. Deville and E. Mund, Chebyshev pseudospectral solution of second-order elliptic equations with finite element pre-conditioning, *J. Comput. Phys.* **60,** 517 (1985).
33. B. Fornberg, *A Practical Guide to Pseudospectral Methods* (Cambridge Univ. Press, New York, 1996).
34. J.-M. Vanden-Broeck, Elevation solitary waves with surface tension, *Phys. Fluids A* **3,** 2659 (1991).
35. J.-M. Vanden-Broeck, Gravity-capillary free surface flows, in *Asymptotics beyond All Orders,* edited by H. Segur, S. Tanveer, and H. Levine (Plenum, New York, 1991), p. 275.
36. R. H. J. Grimshaw and N. Joshi, Weakly non-local solitary waves in a singularly-perturbed Korteweg-deVries equation, *SIAM J. Appl. Math.* **55,** 124 (1995).
37. J. P. Boyd, Multiple precision pseudospectral computations of the radiation coefficient for weakly nonlocal solitary waves, *Comput. Phys.* **9,** 324 (1995).
38. L. M. Delves, Expansion methods, in *Modern Numerical Methods for O. D. E.s,* edited by G. Hall and J. M. Watts (Oxford Univ. Press, Oxford, 1976), p. 269.
39. J. P. Boyd, *Weakly Nonlocal Solitary Waves and Other Exponentially Small Phenomena* (Kluwer, Amsterdam, 1998).
40. M. V. Berry, Asymptotics, superasymptotics, hyperasymptotics, in *Asymptotics beyond All Orders,* edited by H. Segur, S. Tanveer, and H. Levine (Plenum, New York, 1991), p. 1.